Electronic Supplementary Information (ESI) for

Structural Analysis of Micrometer-Long Gold Nanowires Using Wormlike Chain Model and Their Rheological Behavior

Masashi Saitoh*, Yukiyasu Kashiwagi, and Masaya Chigane

Osaka Municipal Technical Research Institute (OMTRI), Osaka 536–8553, Japan

Contact Address: smasashi@omtri.or.jp

(1) A TEM image of AuNW (180 min) before centrifugation

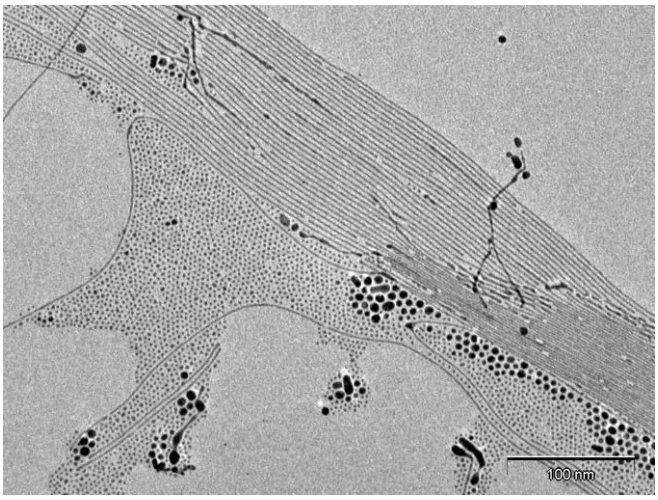

Figure S1 A TEM image of AuNW (180 min) before centrifugation.

(2) Diagrammatic sketch of bundled AuNWs

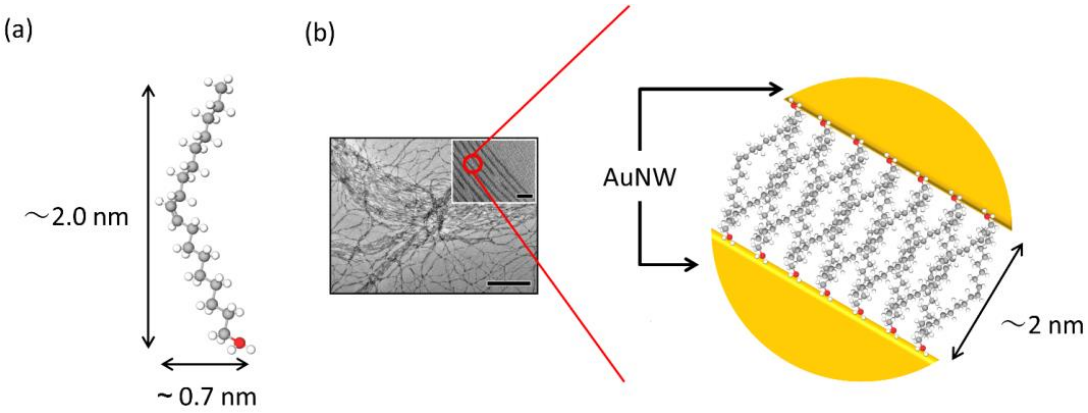

Figure S2. (a) Chemical structure of oleylamine (grey: carbon, white: hydrogen, red: nitrogen). Structural information is based on the reference (S. Mourdikoudis and L. M. Liz-Marzán, *Chem. Mater.*, 2013, **25**, 1465–1476.). (b) Diagrammatic sketch of the surface between AuNWs.

(3) Thermogravimetric analysis (TGA) profiles of the dried AuNWs (60, 90, 180, 360 min)

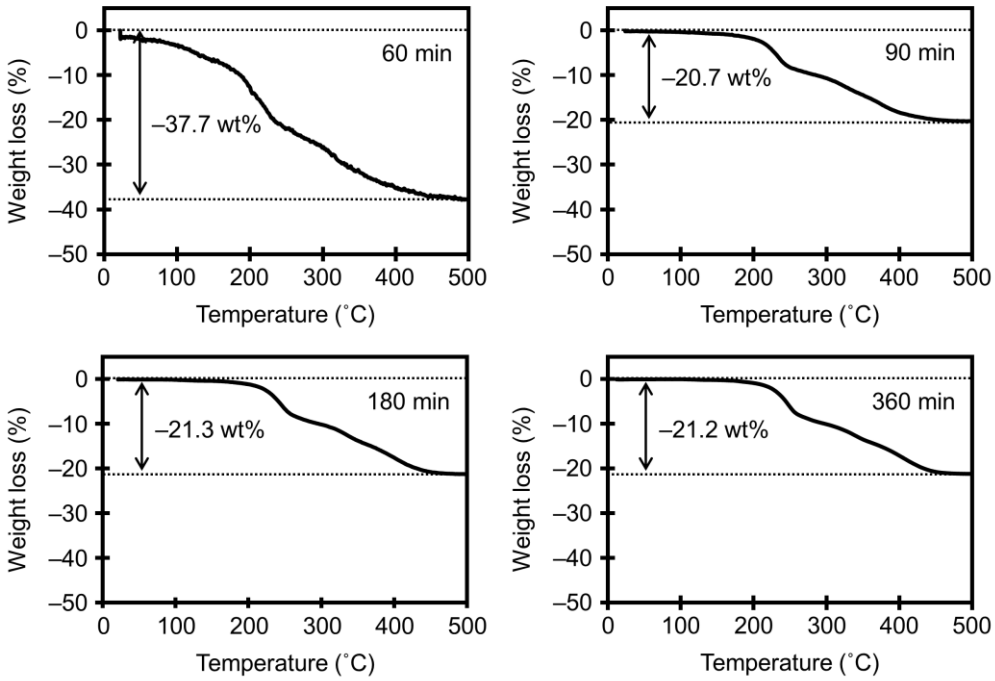

Figure S3. TGA profiles of the dried AuNWs after reaction times of 60, 90, 180, and 360 min. Au contents of each sample were estimated from the weight loss at 500 °C to be 62.3, 79.3, 78.7, and 78.8 wt% for AuNWs of 60, 90, 180, and 360 min, respectively.

(4) Coversion of the reaction on AuNW growth

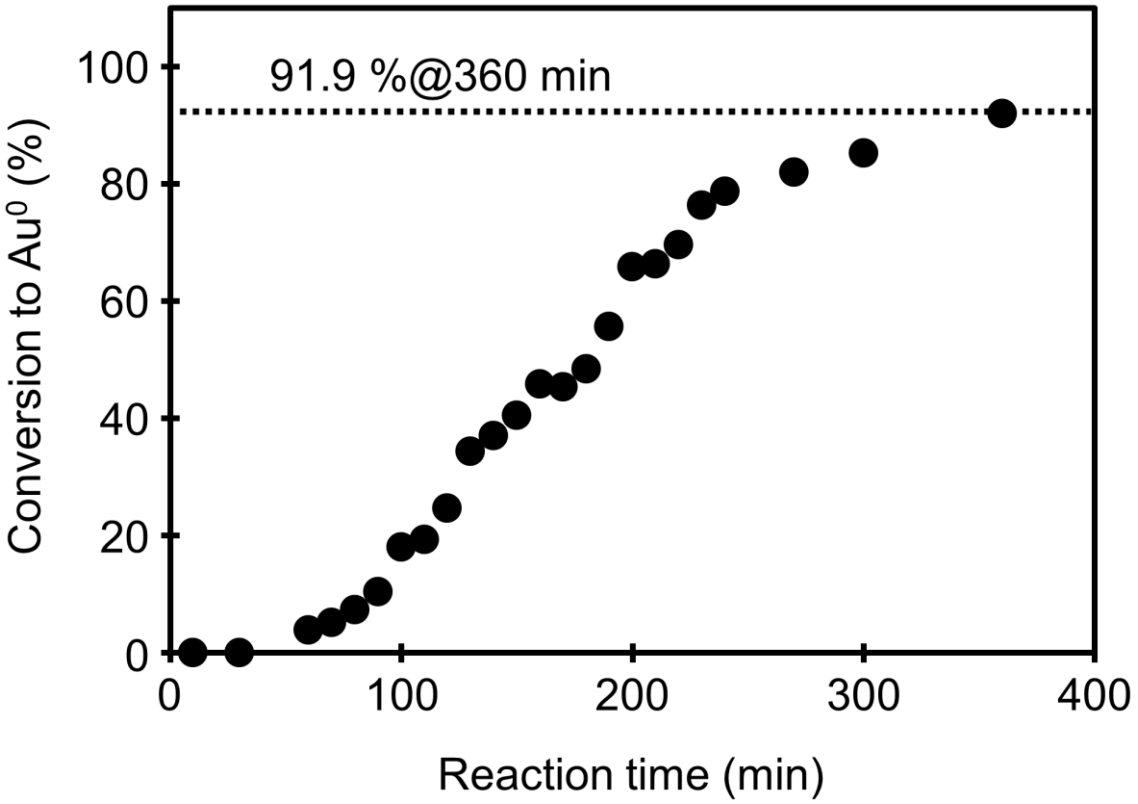

Figure S4. Conversion of Au ions into Au^0 as a function of the reaction time. Reduction of $HAuCl_4$ in *n*-hexane with OLA as a capping ligand was performed by TIPS as a reducing reagent. The conversion reached to be 91.9 % at the raction time of 360 min.

(5) Determination of differential refractive index increment (*dn*/*dc*) of AuNWs after reaction times of 60, 90, 120, 150, 180, 210, 240, 270, 300 and 360 min in *p*-TBT using an Abbe refractometer

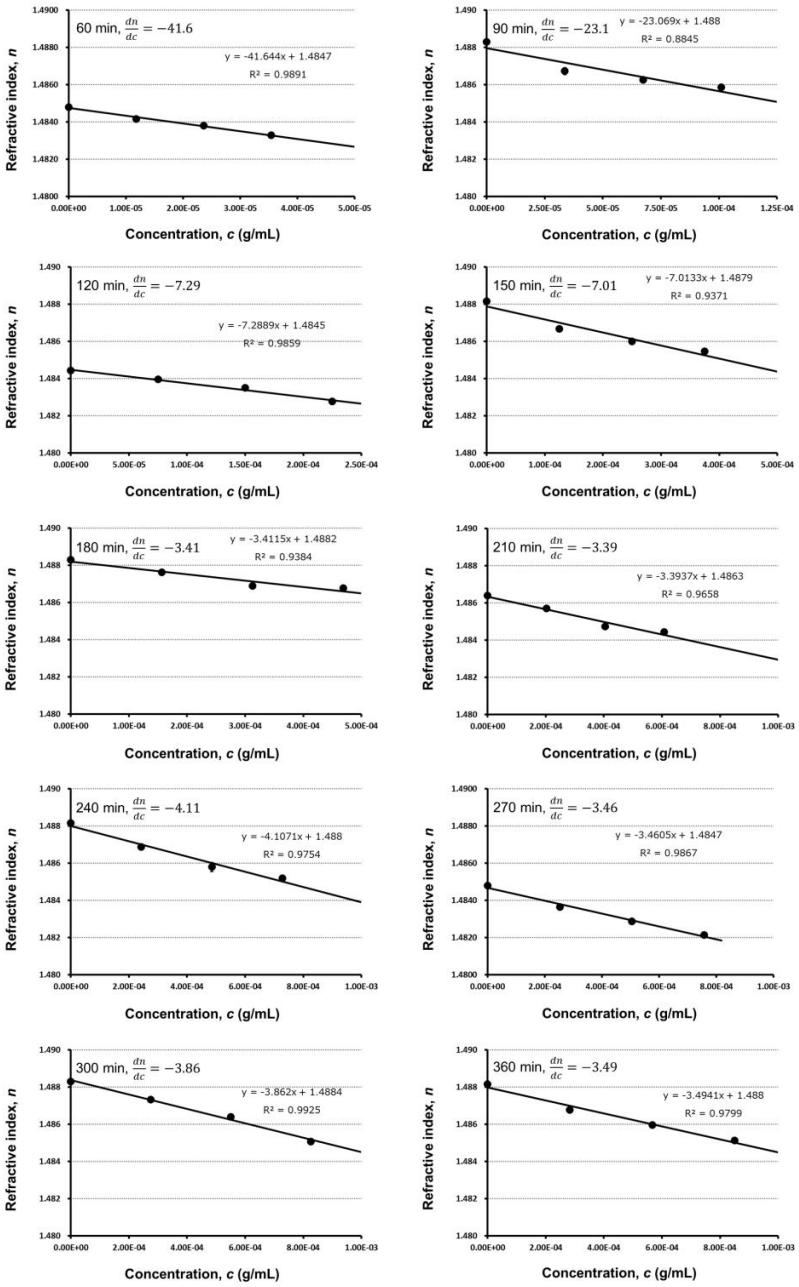

Figure S5. Plots of refractive index (*n*) as a function of the sample concentration (*c*) of AuNWs after reaction times of 60, 90, 120, 150, 180, 210, 240, 270, 300, 360 min in *p*-TBT. Symbols indicate observed data and solid lines are fitting lines based on the linear function. The differential refractive index increments (*dn*/*dc*) were estimated from the slopes of the fitting lines which are evaluated by the least-squares method and are given in each figure.

(7) Derivation of the developed Sharp–Bloomfield (S–B) equation, $P_z(q)$ (equation 3)

Assuming the monodisperse system, the formula for angular distribution of light scattered by a object of flexible chain is presented by the Sharp–Bloomfield (S–B) equation given below:

$$P(q) = \frac{2}{(Lb)^2}\frac{1}{k^2}(e^{-kLb} + kLb - 1) + \frac{b}{L}\left\{\frac{4}{15} + \frac{7}{15kLb} - \left(\frac{11}{15} + \frac{7}{15kLb}\right)e^{-kLb}\right\} \quad \text{(S1)}$$

in equation S1,

$$k = \frac{q^2}{6}$$

with scattring vector of

$$q = \frac{4\pi n}{\lambda}\, sin\frac{\theta}{2}$$

where L, b, θ, and n are contour length, the Kuhn length, angle of scattered light, and refractive index of solvent, respectively. The first term of the equation S1 is well known as the Debye function.

For the polydisperse system obeying the Schulz–Zimm distribution of chain length, the equation S1 is developed to be of integral form:

$$P_z(q) = \int_0^\infty L\, w(L)\, P(q)\, dL \Big/ \int_0^\infty L\, w(L)\, dL \quad \text{(S2)}$$

with the Schulz–Zimm distribution function of

$$w(L) = \frac{y^{z+1}}{z!}\, L^z\, e^{-yL}$$

in this function,

$$y = \frac{z+1}{L_w}$$

and

$$z = \frac{1}{L_w/L_n - 1}$$

here z, L_w, L_n are dispersion parameter, weight-average contour length, and number-average contour length, respectively. For the chain with monodiperse length, z is defined as infinity, whereas z decreases for the chain with polydiperse length. By introducing the equation S1 into the equation S2, calculation of each integral component is derived to be equation S3 and S4:

$$\int_0^\infty L\, w(L)\, P(q)\, dL = \int_0^\infty L\, \frac{y^{z+1}}{z!}\, L^z\, e^{-yL}\left[\frac{2}{(Lb)^2}\frac{1}{k^2}(e^{-kLb} + kLb - 1) + \frac{b}{L}\left\{\frac{4}{15} + \frac{7}{15kLb} - \left(\frac{11}{15} + \frac{7}{15kLb}\right)e^{-kLb}\right\}\right] dL$$

$$= \frac{y^{z+1}}{z!}\left[\frac{2}{b^2}\frac{1}{k^2}\int_0^\infty \left\{L^{z-1}\,e^{-(y+kb)L} + kbL^z\,e^{-yL} - L^{z-1}e^{-yL}\right\} dL\right.$$

$$\left. + \frac{b}{15}\int_0^\infty \left\{4L^z e^{-yL} + \frac{7}{kb}L^{z-1}e^{-yL} - 11L^z e^{-(y+kb)L} - \frac{7}{kb}L^{z-1}e^{-(y+kb)L}\right\} dL\right]$$

$$= \frac{y^{z+1}}{z!}\left[\frac{2}{b^2}\frac{1}{k^2}\left\{\frac{(z+1)!}{(y+kb)^z} + kb\,\frac{z!}{y^{z+1}} - \frac{(z-1)!}{y^z}\right\}\right.$$

$$\left. + \frac{b}{15}\left\{\frac{4\,z!}{y^{z+1}} + \frac{7}{kb}\,\frac{(z-1)!}{y^z} - \frac{11\,z!}{(y+kb)^{z+1}} - \frac{7}{kb}\,\frac{(z-1)!}{(y+kb)^z}\right\}\right]$$

$$= \frac{y}{z}\left[\frac{2}{b^2}\frac{1}{k^2}\left\{\frac{1}{\left(1+\frac{kb}{y}\right)^z} + kb\,\frac{z}{y} - 1\right\}\right.$$

$$\left. + \frac{b}{15}\left\{\frac{4\,z}{y} + \frac{7}{kb} - \frac{11\,z}{y+kb}\,\frac{1}{\left(1+\frac{kb}{y}\right)^z} - \frac{7}{kb}\,\frac{1}{\left(1+\frac{kb}{y}\right)^z}\right\}\right]$$

substituting $y = \frac{z+1}{L_w}$ into the above formula leads the equation S3 as follow:

$$\begin{aligned}\int_0^\infty L\,w(L)\,P(q)\,dL &= \frac{2}{z\,\frac{L_w\,b^2}{z+1}}\,\frac{1}{k^2}\left\{\frac{1}{\left(1+\frac{L_w b}{z+1}\right)^z} + z\,\frac{L_w b}{z+1}\,k - 1\right\}\\ &\quad + \frac{b}{15}\left[4 + \frac{1}{z\,\frac{L_w b}{z+1}\,k} - \left\{\frac{11}{1+\frac{L_w b}{z+1}} + \frac{7}{z\,\frac{L_w b}{z+1}\,k}\right\}\frac{1}{\left(1+\frac{L_w b}{z+1}\right)^z}\right]\end{aligned} \tag{S3}$$

$$\begin{aligned}\int_0^\infty L\,w(L)dL &= \int_0^\infty L\,\frac{y^{z+1}}{z!}\,L^z\,e^{-yL}\,dL = \frac{y^{z+1}}{z!}\int_0^\infty L^{z+1}\,e^{-yL}\,dL\\ &= \frac{y^{z+1}}{z!}\cdot\frac{(z+1)!}{y^{z+2}} = \frac{z+1}{y}\end{aligned}$$

substituting $y = \frac{z+1}{L_w}$ into the above formula leads the equation S4 as follow:

$$\int_0^\infty L\,w(L)dL = L_w \tag{S4}$$

For derivation of the equation S3 and S4, the following integral formula is used:

$$\int_0^\infty x^\alpha\,e^{-\beta x}\,dx = \frac{\alpha!}{\beta^{\alpha+1}}$$

Taking into account by incorporating the equation S3 and S4 into the equation S2, the developed Sharp–Bloomfield (S–B) equation, $P_z(q)$ (equation 3 in the literature), is evetually derived.

(8) Contour length of AuNWs as a function of reaction time

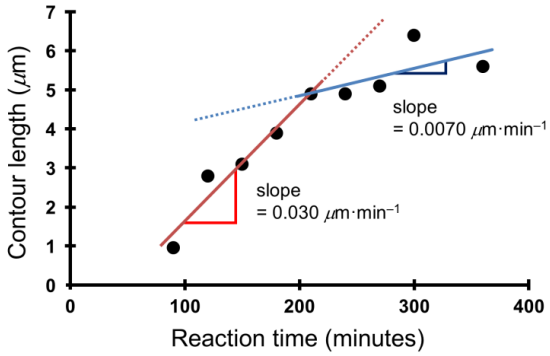

Figure S6 Contour length as a function of reaction time. Solid lines represent the best-fit lines by a least-square method. The growth rate of AuNWs was estimated to be 0.030 μm· min^{-1} (90–210 min) and 0.0070 μm· min^{-1} (210–360 min) respectively.

(9) Determination of crystalline domain size of AuNW (360 min) using Scherrer's equation

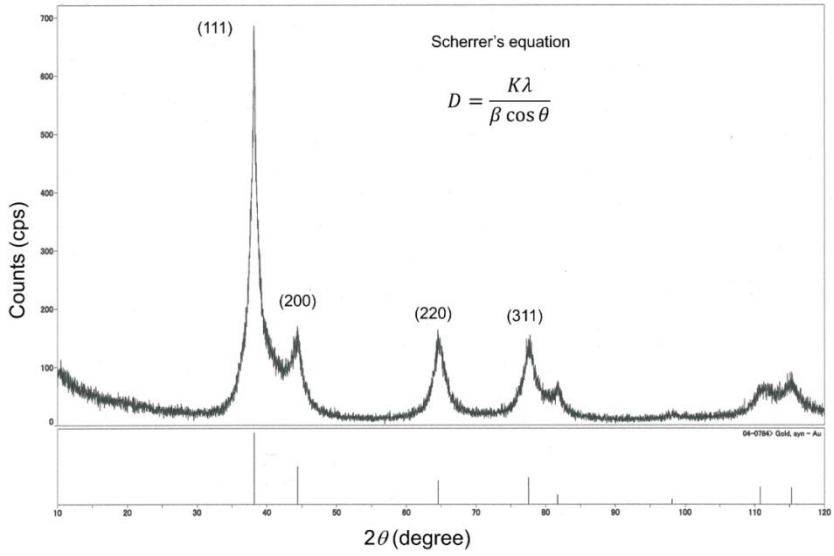

Figure S7. X-ray diffraction (XRD) pattern of AuNW (360 min). The (fcc) structure of AuNWs was confirmed. The XRD peaks at 38.2˚, 44.4˚, 64.6˚ and 77.6˚ were assigned as (111), (200), (220) and (311) reflection lines, respectively, which were in agreement with the diffraction standard of Au (JCPDS 04–0784 represented as vertical bars at the bottom). For estimation of crystalline domain size (D), the Scherrer's equation was adapted with shape factor, K = 0.94 for spherical shape, X-ray wavelength, λ = 0.154 nm, broadening of half of the maximum intensity in radian, β = 0.020 rad, and Bragg angle, θ = 19.1˚, resulting the crystalline domain size, D of 7.7 nm was obtained.

(10) TEM observation of AuNW (360 min) stored for a month

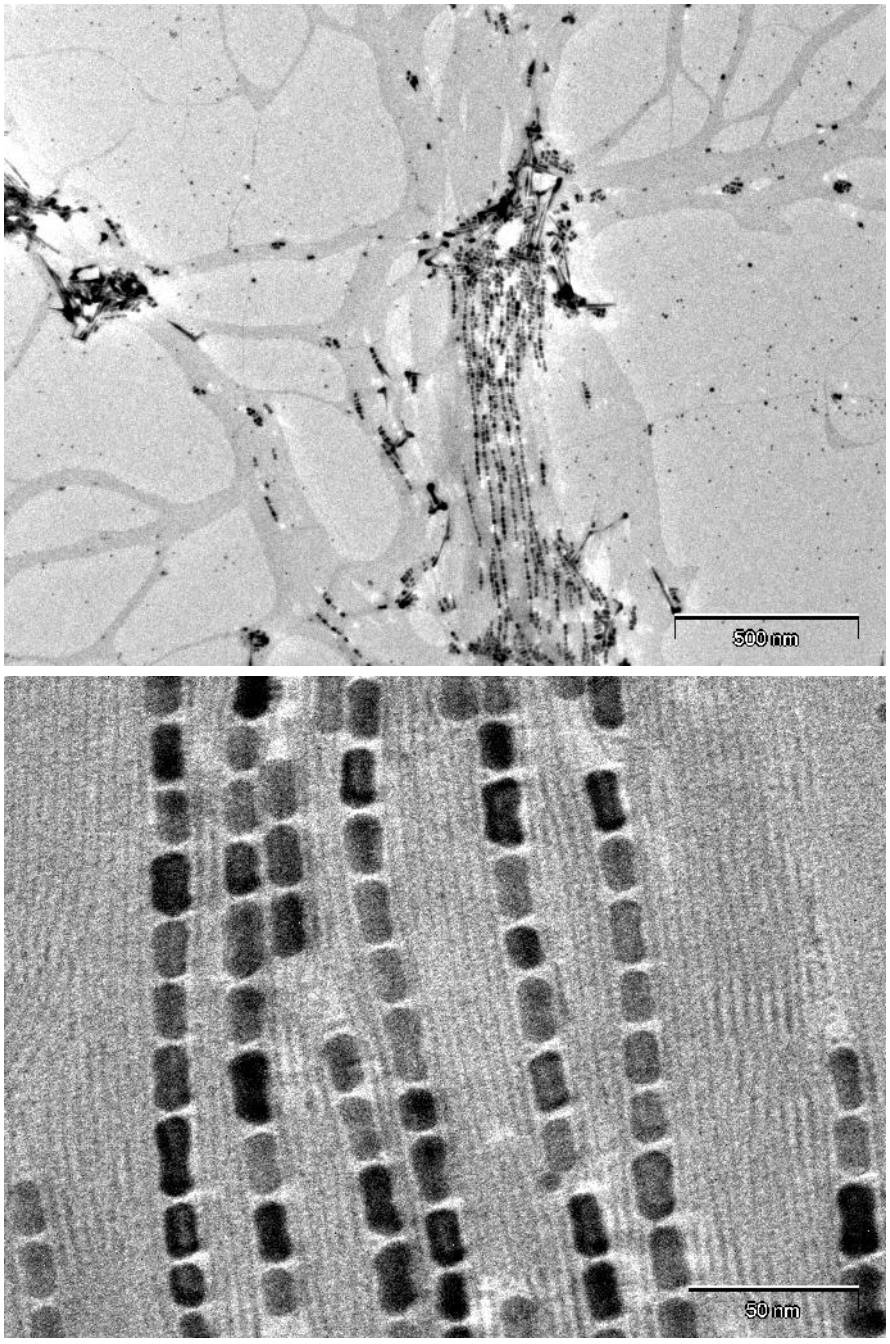

Figure S8. TEM images of AuNW (360 min) stored as toluene solution for a month. (Top) Crystallite domains of AuNWs partially grew much bigger though the shape was maintained in most of the part of the TEM view. (Bottom) Cylindrical form objects were observed, in which Rayleigh instability process may occur.

(11) TEM of the oleylamine capped AuNP (OLA–AuNP)

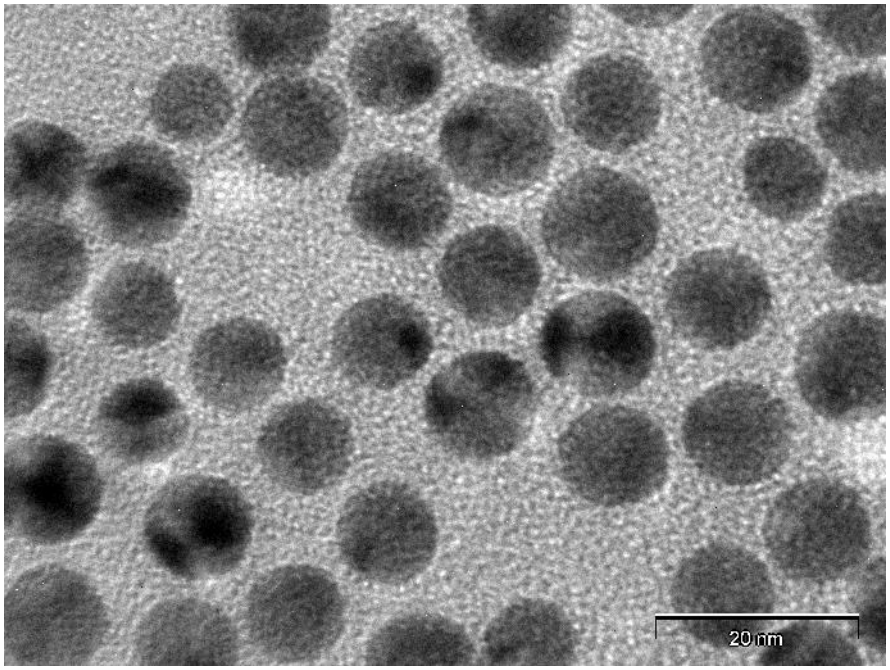

Figure S9. A TEM image of OLA–AuNP. The average core diameter size of 8.7±1.0 nm was observed, based on the analysis of 50 nanoparticles.